

CONSISTENT OPERATION OF THE HOUGHTON COLLEGE

DEPOSITION CHAMBER

By

Jared M. Malone

A thesis submitted in partial fulfillment of the requirements for the
degree of

Bachelor of Science

Houghton College

June 7th, 2021

Signature of Author.....

Department of Physics
June 7th, 2021

.....

Dr. Brandon Hoffman
Professor of Physics
Research Supervisor

.....

Dr. Mark Yuly
Professor of Physics

**CONSISTENT OPERATION OF THE HOUGHTON COLLEGE
DEPOSITION CHAMBER**

By

Jared M. Malone

Submitted to the Department of Physics
on June 7th, 2021 in partial fulfillment of the
requirement for the degree of
Bachelor of Science

Abstract

An apparatus constructed to consistently and systematically deposit thin metal films using thermionic emission has been refined. A turbo pump lowers the base pressure of the deposition chamber to 10^{-6} Torr. Thermionic emission is achieved via current passing through a tungsten filament that is held at -4 kV relative to the desired deposition material. Multiple refinements were made to the apparatus' high voltage circuit to improve the consistency of operation, primarily the securing of multiple connections within the circuit. Additionally, two 2 kV microwave transformers, and four diodes used to produce a doubling rectifier were replaced, and a capacitor bank was added to further refine the output of the forementioned circuit. While production of a thin metal film has yet to be achieved, the high voltage power supply is capable of consistently maintaining a high negative potential to facilitate the production process. Future work and modifications of the apparatus are also discussed.

Thesis Supervisor: Dr. Brandon Hoffman
Title: Professor of Physics

TABLE OF CONTENTS

Chapter 1 History..... 5
 1.1. Vacuum 5
 1.2. Evaporation of Metals..... 7
 1.3. Research in Thin Films and Their Production 9
 1.3.1. Thin Films 9
 1.3.2. Miller Indices and Atomic Structure..... 10
 1.3.3. Thin Film Texture 11
 1.3.4. Film Production at Houghton College 13
Chapter 2 Theory 14
 2.1. Thermionic Emission 14
 2.2. Deposition Rate..... 18
 2.3. Deposition Rate Monitor 20
 2.4. High Voltage Circuit..... 21
 2.4.1. Circuit Overview..... 21
 2.4.2. Transformers..... 21
 2.4.3. Half Wave Voltage Doubler 23
Chapter 3 Apparatus..... 26
 3.1. Deposition Chamber..... 26
 3.1.1. Vacuum System..... 26
 3.2. High Voltage Circuit..... 26
 3.3. Chamber Interior 28
 3.3.1. Filament..... 28
 3.3.2. Crucible..... 29
 3.3.3. Deposition Rate Monitor 29
 3.3.4. Sample Holder 30
 3.3.5. Motion Feedthroughs 30
Chapter 4 Conclusion 31
 4.1. Chamber Operability..... 31
 4.1.1. Substrate Temperature Control 31
 4.1.2. Deposition Rate Monitor 31
 4.1.3. Linear Shutter..... 32
References..... 33

TABLE OF FIGURES

Figure 1. Sprengel's Apparatus.....	6
Figure 2. Image of internal mechanisms of a turbopump	7
Figure 3. Diagram of a graphite crucible.....	9
Figure 4. Visual representation of the crystal cubic system	10
Figure 5. Visual representations of the two common orientations of crystals in silver..	11
Figure 6. Stacking formation of ideal crystal and crystal with stacking faults	13
Figure 7. Diagram of thermionic emissions apparatus	14
Figure 8. Diagram of Deposition Rate Geometry.....	19
Figure 9. Diagram of High Voltage Circuit.....	21
Figure 10. Isolated image of both half wave voltage doublers.....	24
Figure 11. Plot of ideal doubler output	24
Figure 12. Plot of ideal half wave voltage doubler output.	25
Figure 13. Diagram of ideal output of capacitor bank.	25
Figure 14. Image of the exterior of the deposition chamber.....	27
Figure 15. Diagram of the interior of the deposition chamber.	27
Figure 16. Image of filament.....	28
Figure 17. Image of crucible and ceramic stand.	29
Figure 18. Images of deposition rate monitor.....	29
Figure 19. Image of Sample Holder.....	30

Chapter 1

HISTORY

1.1. Vacuum

Vacuums are fundamental in the deposition process and the construction of thin metal films. It is through the presence of a vacuum that we are more capable of producing pure thin metal films with minimal impurities. Due to their fundamental importance in the production of thin metal films the history of vacuums will be discussed in the following section.

Vacuums have been a fascination of mankind since the 17th century. In 1677 the German scientist Otto Von Guericke [1] discussed the idea of a vacuum saying, "it is impossible to make or render space empty in an ideal sense. Nevertheless, it does not follow from this that a vacuum does not exist in nature...". Von Guericke conducted several experiments showing that an unideal vacuum could be produced and analyzed the vacuums properties. It was noted that an object containing a vacuum has an incredible amount of force exerted upon it by the external air pressure of the atmosphere. Additionally, it was observed that when water was subject to the evacuation of air, the water began to boil at room temperature. The increased evaporation of water at room temperature in the presence of a vacuum was fundamental as it suggested that substances exposed to a vacuum would require less energy to evaporate. Vacuums were further researched by Dr. Hermann Sprengel in 1865, who developed an improved apparatus, see Figure 1, to produce a vacuum. Sprengel [2] utilized falling mercury to syphon off air in container, thus producing a vacuum. Many of Von Guericke's apparatuses centered around a pump design, utilizing the displacement of water to produce a vacuum.

Since the 18th century multiple methods have been developed to produce vacuums such as diffusion pumps, ion pumps, and rotary vane pumps. Diffusion pumps and turbomolecular pumps both function through momentum transfer. Diffusion pumps operate by a jet of vapor, flowing from the intake portion of the pump to exhaust. The chosen molecules

diffuse into the vapor with the flow of the jet and thus become expelled [3]. Diffusion pumps can achieve pressures around 10^{-6} Torr. Ion pumps function through electrical discharge. The area that is to be evacuated is ionized and strikes the cathode of the ion pump which then evacuates the gas by chemisorption or physisorption, thereby producing a vacuum [4]. Modern versions of these devices can reach pressures as low as 10^{-11} Torr [5].

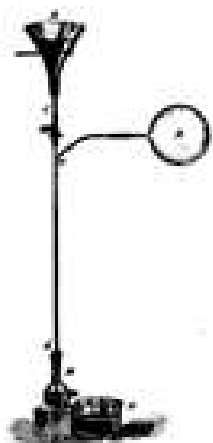


Figure 1. Sprengel's Apparatus. Mercury is poured into a funnel A, falls down the tube from C to D producing a vacuum in R, and empties out through the spout at B into the beaker H. Image taken from Ref. [2].

The rotary vane pump is a mechanical pump composed of a circular rotor inside an encompassing circular cavity, the rotor is offset from the center of the circular cavity. Early versions of a mechanical pump were constructed in 1909 and in 1966. Wolfgang Gaede developed an "apparatus for producing high vacuum". The device, a turbomolecular pump, utilized the friction between the evacuated gas and the walls of the pump to force the gas out of the desired chamber. Becker developed a turbo pump allowing for a more sustainable and intense vacuum with vacuums being formed with a pressure of 10^{-8} Torr. The device uses a rotor containing vanes that can move in and out of the rotor such that a seal is maintained along the outer cavity throughout the rotation of the rotor. The Rotary vane pump utilizes the change in volume of the vanes between the intake and exhaust sides of the pump to force fluid into the exhaust, seen in Figure 2. These types of pumps can produce pressures of 10^{-6} Torr.

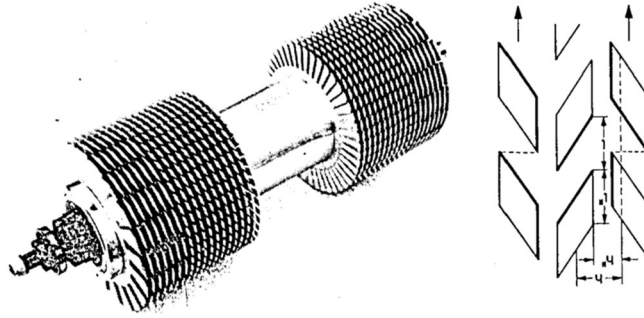


Figure 2. Image of internal mechanisms of a turbopump. Developed by Becker. This Turbo pump functions through a series of metal fans propelling gas out of the desired location. A cross section of the blades is shown in the right image. The blades act like a series of inclined planes sliding past each other such that air is moved out of the desired area. Images taken from Ref. [6].

The modern turbomolecular pump functions through a rotor attached to a series of angled blades in an enclosed cylinder, the rotor spins the blades imparting momentum to the desired molecules funneling them out to the exhaust of the pump, producing a vacuum at the intake section of the pump. In the proper conditions turbomolecular pumps can reach pressures of 10^{-11} Torr.

This history brings us to the present of chamber evacuation which is utilized in film deposition. Turbopumps similar in function to the devices described above are utilized in the process of metal evaporation, in order to decrease the presence of impurities.

1.2. Evaporation of Metals

Thin films are produced using a variety of methods including electroplating, spin coating, sputtering, and electron beam evaporation. Electroplating is the process of using electrical current to plate a metal solution on a cathode of a circuit. The first documentation of electroplating was of Professor Luigi Brugnatelli, who used electroplating to produce a thin film of gold over silver metal [7]. The electroplating process is relatively inexpensive as no vacuum is required, and film thickness can be controlled precisely [8]. However, the process is relatively time intensive for an undergraduate level project. As such, electroplating is not the method used for the production of Houghton College is thin films.

The process of producing thin films through spin coating was first discussed in 1958 by Alfred G. Emslie [9]. Spin coating utilizes a solution applied to a substrate that is spun in a

centrifuge to produce the film. The process is relatively simple and can produce consistent films with a relatively low cost. However, spin coating requires that the substance being deposited is a fluid and actual material usage is low causing a degree of waste in valuable materials [10].

Chemical vapor deposition utilizes various chemical reactions to produce evaporation of the desired substance which is then deposited onto a substrate. Chemical vapor deposition was first utilized by Sawyer and Man in 1880 with the deposition of carbon on lamp filaments [11]. While this process has a similar methodology of physical deposition, chemical vapor deposition frequently produces volatile byproducts that could potentially cause harm to the operator.

The first physical vapor deposition of metal into a thin film was in 1921 by Kahler [12]. Kahler evaporated bismuth, silver, and several other metals in tubes, via sputtering. The metals' physical properties were then studied and recorded via x-ray powder method as developed by Debye and Scherrer. Since then, several methods for constructing thin films have been developed.

In 1934 O'Bryan [13] discussed the method of evaporating metal substances that are contained in a crucible that is surrounded by a powered filament. Some of the methods previously used had involved direct contact with the substance to be evaporated. The substance was heated via direct contact with a heated filament. However, this proved incredibly inefficient as the heating element was at a much higher temperature than the evaporating substance. The new method developed by O'Bryan allowed for the evaporation of substances with a relatively high evaporation temperature as the temperature difference between the filament and the substance were drastically reduced. An image of the apparatus is shown in Figure 3.

In 1960 Giedd and Perkins [14] developed an evaporation rate monitor utilized in the construction of thin films. The monitor functioned by measuring the amount of ionization occurring within the system, which was found to be dependent upon evaporation rate. The device uses a powered filament surrounded by a cylindrical anode to ionize the desired

substance. The current output of the device was therefore proportional to the amount of ionization. With such a device, films of a specified thickness could now be constructed thereby allowing for more controlled research into the physical properties of thin films.

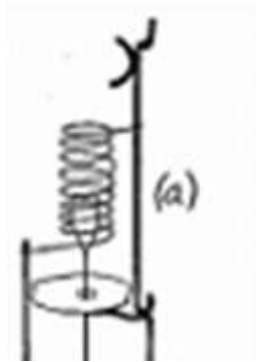


Figure 3. Diagram of a graphite crucible . The crucible holds the desired substance suspended by a tungsten filament of 1 mm in diameter. The heliacal filament surrounding the crucible is also made of tungsten and is provided with a potential to heat the substance. Image taken from Ref. [13]

1.3. Research in Thin Films and Their Production

1.3.1. Thin Films

A thin film is any substance formed such that one dimension is significantly smaller than the other two or whose thickness is on the order of grain size. And there has been interest in their microstructure and the resulting properties thereof. Thin films have multiple applications in many fields including interface filters, polarizers, narrowband filters, solar cells, photoconductors, IR detectors, wave drive coatings, and temperature control within electronics. As the microstructure of a thin film changes, physical properties of the film also change such as susceptibility to stress and strain and thermal and electrical conductivity. When the microstructure of a thin metal film is subject to stress it will transform and alter its structure. This process is known as transformation. Transformation has been observed as early as 1966 by C.G. Dunn and J.L. Walter [15]. In thin silver films, it has been well documented [17-22] that a film transforms from (111) orientation to (100) orientation after annealing when the thickness of film exceeds one micrometer. Similarly, it has been

documented [19] that thin films composed of gold transform. Gold grains undergo growth in the annealing process, and the movement of grain boundaries is recorded.

As such being able to understand the forces behind these transformations would have a positive impact device that utilize films in conditions where transformation is possible. However, there are two main issues complicating the research process of these films. The present goal of thin film research is to determine the driving force of texture transformation. For complete research to be conducted on texture transformation several variables must be recorded. Time, film thickness, and deposition temperature have all been found to effect texture transformation and research containing all these variables is rare. The second complication is the presence of impurities in thin films. Grain structure is highly susceptible to the presence of impurities as such environmental factors should also be recorded. An additional problem is that only one type of film for a given set of variables can be made in each run of the film construction process. As a result, the construction of enough films to conduct a complete and thorough study is both costly in time and resources.

1.3.2. Miller Indices and Atomic Structure

It is necessary to discuss the atomic structure of metals before further discussing transformation. There are many structures of thin films; one of the possible structures of a thin film is described using a crystal cubic system, which consist of primary cubic (simple cubic), body-centered cubic (bcc), and face-centered cubic (fcc), as depicted in Figure 4.

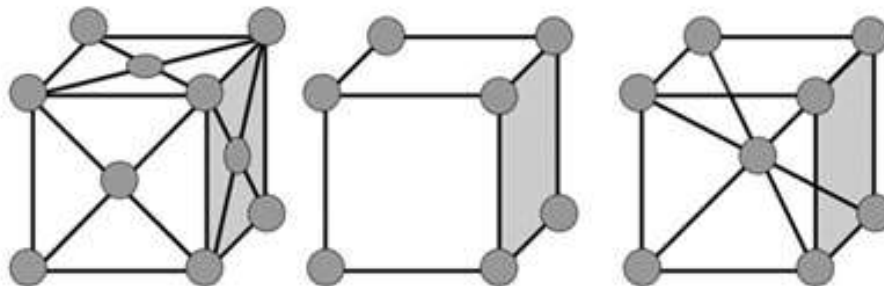


Figure 4. Visual representation of the crystal cubic system . From left to right, primary cubic (simple cubic), body-centered cubic (bcc), and face-centered cubic (fcc).

As an example, silver's atomic structure is face-centered cubic where the geometric pattern shown in is repeated in certain orientations. Orientation refers to how the atoms of silver position themselves relative to a surface and can be described by a notation known as Miller indices. These indices are used to denote the direction of the normal vector describing the plane that is parallel to the plane formed by the film surface. Miller indices are in crystal coordinates. The two most common orientations in silver are (100) and (111) shown in Figure 5. It is important to note that there are multiple types of crystal coordinates and not all thin films are of crystalline structure, however the example silver's miller indices are useful for discussing transformation.

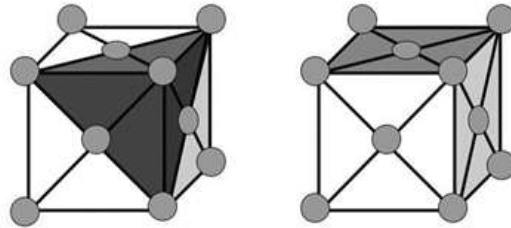


Figure 5. Visual representations of the two common orientations of crystals in silver. Highlighted planes are parallel to substrate. (111) orientation is depicted on the left, (001) or (100) right.

1.3.3. Thin Film Texture

The texture of a thin film refers to the dominant orientation or the crystal grains. A texture is said to be “strong” if nearly all of volume of the film is composed of grains with a given orientation. After a film has been constructed with the deposition chamber one can observe texture transformation within the film. Texture transformation is when the texture of the film changes over time. This change occurs due to growth of grains with a non-dominant orientation. These grains may have existed in the film of grains that nucleated during the transformation process. This transformation of texture has been observed in multiple thin metal films, such as silver, gold, and nickel [15, 16]. Transformation can change properties on a macroscopic scale, such as resistance, thermal conductivity, hardness, even the saturation magnetization [17]. However, the driving force behind thin film transformations is still unknown.

One early hypothesis regarding thin film transformation is that it is driven by the minimization a surface and interface energy within the film [16, 18, 20]. The model suggests that texture transformation is a result of competition between anisotropic interface and strain energy. Specifically referring to silver, we observe that the (111) orientation has the lower interface energy compared to the (100) orientation. However, the (100) orientation has a lower strain energy for a given elastic strain. It has been observed [18] that at a constant elastic strain the interface energy per unit volume remains constant as film thickness changes, whereas the interface energy per unit volume decreases as an inverse of film thickness. Under this model there should exist a film thickness, under which the film should adopt an overall (111) orientation to minimize interface energy, and over which the film adopts an overall (100) orientation to minimize stress energy. This model, however, fails to account for cases where [19] transformation has occurred in films regardless of the density of interface energy per unit volume. Additionally, recent work has called this hypothesis into question as interface energy does not appear to play a dominant role in texture transformation [20].

One additional hypothesis regarding thin film transformation is that it is driven by the minimalization of twin boundaries [18]. Twin boundaries are crystal boundaries that form due to an intersection between two growing crystal grains, as depicted in Figure 6. It is known that transformation can be driven by the reduction of defect energy which is produced by grain boundaries and stacking faults. As grain growth occurs total grain boundary energy and thus defect energy decrease. It is important to note that this model does not predict a thickness dependence, with thinner films not transforming.

It is this ambiguous understanding of the driving force of transformation that motivates research within the area of thin films. A better understanding of thin-film transformation is desirable for the improved manufacturing of thin films and devices that use them. As such, it is necessary to be able to produce multiple films with a variety of conditions. This necessity can be filled by the production and maintenance of a deposition chamber, which would allow for the construction of various thin metal films for research purposes.

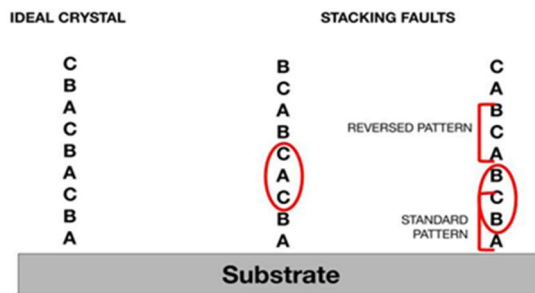


Figure 6. Stacking formation of ideal crystal and crystal with stacking faults. Layers A B C refer to matching planes parallel to substrate formed by Ag atoms. Note that after a stacking fault occurs the stacking order is reversed.

1.3.4. Film Production at Houghton College

The faculty and students at Houghton college have had past success in analyzing the properties of thin metal films in collaboration with Cornell University [18]. However, Houghton college is not capable of producing or analyzing thin films locally. To begin the production of thin film's locally, a deposition chamber has been constructed for such a purpose. The deposition chamber at Houghton college utilizes thermionic emission by containing our chosen metal in a graphite crucible in a vacuum suspended above a filament held at a high negative potential. The filament when powered then generates electrons that bombard the crucible containing the metal, resulting in an increase in temperature and ultimately the evaporation of the metal. This method of thermionic emission was ultimately chosen for the ease of use of an undergraduate student as other methods, such as spin coating or chemical vapor deposition are relatively complex processes. A substrate is then mounted above the crucible for the metal to be deposited on. Additionally, during the deposition process the entire chamber is evacuated via a turbomolecular pump and a fore pump. While an ion pump may be more effective in achieving lower pressures of the deposition chamber, a turbomolecular pump was chosen for its ease of operation. By evacuating the chamber during the deposition process one can construct a purer and more uniform film. It is hoped that with sufficient time and resources put toward its construction that the deposition chamber will allow Houghton College to produce thin films for further research.

Chapter 2

THEORY

2.1. Thermionic Emission

The sole method by which the crucible is heated is through thermionic emission. After enough energy is imparted to the crucible and the metal contained within, the deposition process starts to occur, through the evaporation of the metal. Thermionic emission is the process in which electrons are freed from an electrode due to the temperature of said electrode. The apparatus which undergoes thermionic emission is depicted in

Figure 7.

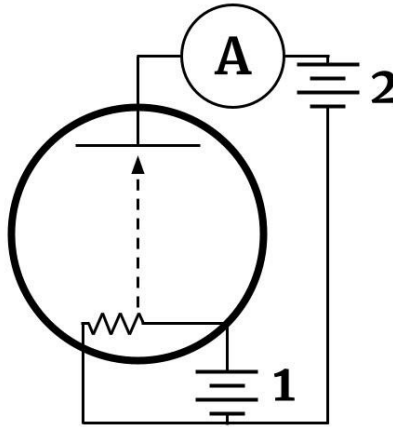


Figure 7. Diagram of thermionic emissions apparatus. Current is supplied to the filament, by power supply 1, within a vacuum resulting in an increase in temperature of the filament. The filament is held at negative potential by power supply 2. Electrons are then freed from the filament and are drawn towards the anode towards ground.

The fundamental idea behind thermionic emission is that all the electrons that have energies greater than the work function W escape from the surface when a metal is at an elevated temperature. The potential energy of an electron a distance z from an infinite, uncharged, conducting plane is:

$$e\Phi = -e\phi + W - \frac{e^2}{16\pi\epsilon_0 z} - e\epsilon z \quad (2.1)$$

where e is the charge of an electron, W is the work function of the conductor, ϕ is the potential of the conductor, ϵ_0 is the permittivity of free space, and ϵ is the magnitude of an applied field that points toward the conductor. The first term on the right is the Fermi level, E_F , of the conductor. The third term on the right is due to the attraction force of the conducting plane on the electron. This results in the position of maximum potential energy:

$$z_{max} = \sqrt{\frac{e}{16\pi\epsilon_0\epsilon}} \quad (2.2)$$

This distance is typically on the order of nanometers, so even a small filament wire, like the one contained in the apparatus, can be reasonably approximated as an infinite plane. Note the magnitude of the applied field in Equation (2.1) is directly dependent on the potential difference between the filament and the crucible. The corresponding potential energy of the electron at this position is

$$e\Phi_{max} = E_F + W - \sqrt{\frac{e^3\epsilon}{4\pi\epsilon_0}} \quad (2.3)$$

$$e\Phi_{max} \equiv E_F + W_{eff} \quad (2.4)$$

where W_{eff} is the effective work function of the conductor in the applied field, as first described by Walter Schottky. This effective work function is the kinetic energy that an electron at the fermi level must acquire to escape the conductor. So the component of the speed of an escaping electron in the z direction must be at least

$$v_z \geq \sqrt{\frac{2\left(W - \sqrt{\frac{e^3\epsilon}{4\pi\epsilon_0}}\right)}{m}} \quad (2.5)$$

where m is the mass of the electron. Let us first consider the nonrelativistic kinetic energy E vs. wavevector \vec{k} relations of a free electron,

$$E = \frac{\hbar^2 k^2}{2m} \quad (2.6)$$

where \hbar is Plank's constant over 2π , and m is the mass of the electron. This is also equivalent to

$$E = m \frac{(v_x^2 + v_y^2 + v_z^2)}{2} \quad (2.7)$$

where v_i are the components of the electron's velocity in a cartesian coordinate system. The momentum p of the electron is,

$$p = \hbar k = mv \quad (2.8)$$

where p is the momentum of the electron and v is the velocity of the electron. The volume per quantum state is $\frac{(2\pi)^3}{V}$. V is the volume of the metal from which electrons are emitted. The number of states in a given k-space volume is equal to the k-space volume, $dk_x dk_y dk_z$, divided by the k-space volume per state, $\frac{(2\pi)^3}{V}$:

$$dS = \frac{2V dk_x dk_y dk_z}{(2\pi)^3}. \quad (2.9)$$

The factor 2 in Equation (2.9) comes from the fact that each state can be occupied by two electrons of opposite spin. Using Equation (2.8), dk can be written as $\frac{m}{\hbar} dv$. So Equation (2.9) can be written as

$$dS = \frac{2Vm^3 dv_x dv_y dv_z}{(2\pi\hbar)^3}. \quad (2.10)$$

We then find that the number dN of electrons of opposite spins occupying the volume, dV is equal to the number of states multiplied by the probability of that state being occupied.

$$dn(T) = \frac{dN(T)}{V} = \frac{2 \left(\frac{m}{\hbar}\right)^3 f(E) dv_x dv_y dv_z}{8\pi^3} \quad (2.11)$$

where $f(E)$ is the fermi function, this results in

$$f(E) = \frac{1}{1 + e^{\frac{E-E_F}{K_B T}}} \quad (2.12)$$

where K_B is the Boltzmann constant. For $(E - E_{F_0}) \gg K_B T$, $f(E)$ can be approximated as:

$$f(E) = e^{\frac{E_F - E}{K_B T}}. \quad (2.13)$$

Of this density of electrons, $dn(T)$ only those electrons will be emitted normal to the metal surface which have speed, v_z that contributions to the current density of the emitted electrons,

$$dJ = ev_z dn(T) \quad (2.14)$$

such that,

$$dJ = \frac{2ev_z \left(\frac{m}{\hbar}\right)^3 dv_x dv_y dv_z}{8\pi^3} e^{\frac{-(E - E_F)}{K_B T}}. \quad (2.15)$$

By Equation (2.7) we find,

$$dJ = \frac{2ev_z \left(\frac{m}{\hbar}\right)^3 dv_x dv_y dv_z}{8\pi^3} e^{\frac{-m(v_x^2 + v_y^2 + v_z^2)}{2K_B T}}. \quad (2.16)$$

The final current density can then be found by integrating dJ along the following bounds; v_y are from $-\infty$ to ∞ , and v_z from v_{z0} to ∞ . The resulting integral evaluates to the following,

$$J = \frac{2\pi e \left(\frac{m}{\hbar}\right)^3}{8\pi^3} \frac{2K_B T}{m} \frac{K_B T}{m} e^{\frac{-m(v_{z0}^2)}{2K_B T}} \quad (2.17)$$

plugging in for v_{z0} we find,

$$J = \frac{4em\pi K_B^2 T^2}{h^3} e^{\frac{-W + \sqrt{\frac{e^3 \epsilon}{4\pi \epsilon_0}}}{K_B T}}. \quad (2.18)$$

Which we write as [21],

$$J = A_0 T^2 e^{\frac{-W_{eff}}{kT}}. \quad (2.19)$$

Notice that J is exponentially dependent on the temperature of the filament undergoing thermionic emission and on the square root of the potential difference between the filament and the crucible. Also, the energy of the electrons arriving at the crucible is

linearly dependent on this potential difference. Because the material to be evaporated is contained within the crucible, its temperature shares these dependences.

2.2. Deposition Rate

Assuming the desired metal evaporates out radially from the crucible, as shown in

, one can determine the rate at which the metal will be deposited on a substrate. [22] The molar flux of a substance, φ , from the condensed form to its gaseous form is expressed by the Hertz-Knudsen equation, given by

$$\frac{1}{\mathcal{A}_{evap}} \frac{d\mathcal{M}}{dt} \hat{r} = \varphi \hat{r} = \frac{P_e - P}{\sqrt{2\pi MRT}} \hat{r} \quad (2.20)$$

where \mathcal{M} is moles of evaporate, \mathcal{A}_{evap} is the surface area of the evaporate, M is molecular mass of the metal, P_e is vapor pressure of the metal, P is the pressure of the condensed phase, T is the temperature at the evaporating surface, \mathcal{R} is the universal gas constant, and \hat{r} is an arbitrary unit vector pointing radially from the source.

Notice that the vapor pressure of the metal is a function of absolute temperature [21],

$$\log P_e = \frac{A}{T} + B \log T + CT + D. \quad (2.21)$$

Thus P_e can be written as,

$$P_e = e^{\left(\frac{A}{T} + B \log T + CT + D\right)} \quad (2.22)$$

for real valued constants A, B, C, D . Thus, the molar flux of an evaporating substance can be given by,

$$\varphi \hat{r} = \frac{e^{\left(\frac{A}{T} + B \log T + CT + D\right)} - P}{\sqrt{2\pi MRT}} \hat{r}. \quad (2.23)$$

Notice that the rate of moles evaporated is dependent on the surface area of the evaporated substance, \mathcal{A}_{evap} . We may assume the evaporated substance can be approximated as a infinitesimally small sphere of radius da .

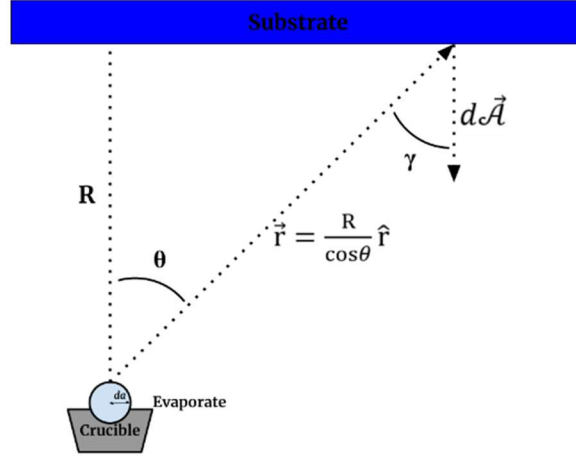


Figure 8. Diagram of Deposition Rate Geometry. r is the distance from the substrate to the crucible, R is the height of the substrate from the crucible, θ is the angle of r from the normal vector of the crucible, and γ is the angle from r from the normal vector of the substrate. Notice given the geometry of the deposition chamber $\gamma = \theta$.

Thus, the rate of evaporation of the evaporate can be described by,

$$\frac{d\mathcal{M}}{dt} \hat{r} = 4\pi(da)^2 \frac{e^{\left(\frac{A}{T} + B \log T + CT + D\right)} - P}{\sqrt{2\pi MRT}} \hat{r}. \quad (2.24)$$

Then the volume evaporated per second, V_{evap} , is found by dividing Equation (2.24) by the molar density of the evaporate, ρ_m . Resulting in,

$$\vec{V}_{evap} = \frac{d\mathcal{M}}{dt} \frac{\hat{r}}{\rho_m} \quad (2.25)$$

$$\vec{V}_{evap} = \frac{4\pi(da)^2}{\rho_m} \frac{e^{\left(\frac{A}{T} + B \log T + CT + D\right)} - P}{\sqrt{2\pi MRT}} \hat{r}. \quad (2.26)$$

The deposition rate, $\frac{dx}{dt}$, where x is the thickness of the deposited film can be determined by,

$$\frac{dx}{dt} = \vec{V}_{evap} \cdot \frac{1}{d\vec{\mathcal{A}}} \quad (2.27)$$

where $d\vec{\mathcal{A}}$ is the infinitesimal area vector of the substrate. We shall assume all of the material evaporated over the substrate sticks to the substrate. Consider the geometry shown in

, where the normal vectors of the substrate and crucible are parallel. R is the height plane of the substrate above the crucible, r is the distance from the substrate to the crucible, θ is the angle from r to the normal vector of the crucible, and γ is the angle of r from the normal vector of the substrate. Thus,

$$d\vec{A} = \left(\frac{R}{\cos\theta}\right)^2 \sin\theta d\theta d\phi \hat{r}_z \quad (2.28)$$

which results in,

$$\frac{dx}{dt} = \frac{4\pi a^2 e^{\left(\frac{A}{T} + B \log T + CT + D\right)} - P \sin\theta}{\rho_m \sqrt{2\pi M \mathcal{R} T} R^2 d\theta d\phi \cos^3\theta} \quad (2.29)$$

So we find that deposition rate is then exponentially proportional to the temperature of the crucible, directly proportional to the square of the radius of the substance, and inversely proportional to the square of the height between the crucible in the substrate.

2.3. Deposition Rate Monitor

The deposition rate monitor within the chamber functions by relating current density to the present rate of deposition. The deposition rate monitor designed by, Giedd and Perkins, [14] is composed of a filament to ionize electrons, a cylindrical accelerating anode, and an ion collector. The ionization probability for molecular beams in this geometry have been calculated to be P . A method for arriving at a value for the ionization probability is to assume the distribution of vapor from a point source. With this assumption we can compare the calculated number of ions to the measured number of atoms deposited on the substrate. P is the maximized ionization probability,

$$P = M I_m \frac{10^{-8}}{N d A \rho e} \quad (2.30)$$

M is molecular mass, I_m is the ion current of the evaporate, N is Avogadro's Number, d is the evaporation rate as determined by a measurement of the thickness of the substrate divided by the total time of evaporation, A is the area of the collector, ρ is the density of the metal, and e is the electronic charge. It has been experimentally determined [14] that the maximum value of ionization probability is $P = 26\%$ for an anode potential of $+155V$, and a collector potential of $-20V$. We may relate I_m to deposition rate by a D by a

proportionality constant α whose value with depend on the substance being evaporated. Thus, deposition rate can be given by,

$$D = \alpha I_m = \alpha \frac{P}{M} NdA\rho e * 10^8 \quad (2.31)$$

2.4. High Voltage Circuit

2.4.1. Circuit Overview

To produce high energy electrons via thermionic emission, the filament must be held at a high negative potential. This is done by floating the filament with a high voltage circuit that produces a reasonably constant negative potential. The circuit diagram is shown Figure 9.

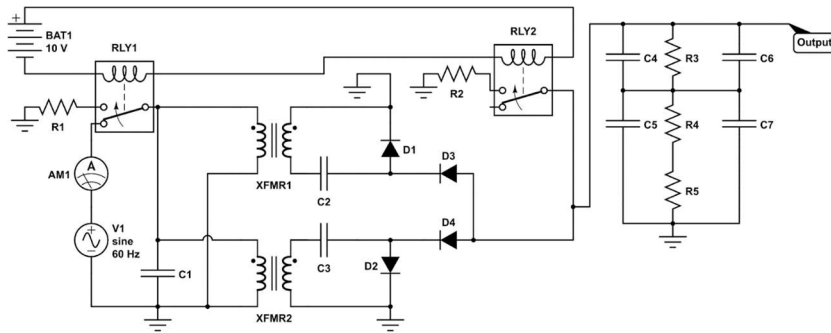


Figure 9. Diagram of High Voltage Circuit. V1 provides 120 V AC at 60 Hz to XFMR 1&2, whose voltage ratio are 1:20. C1-7 are $1 \mu\text{F}$ and functions to adjust the power factor of the transformers. The input of XFMR 1 is wired such that is out of phase with XFMR 2 by π to produce a more consistent voltage output. The transformers outputs are then rectified and doubled through D1-4 and C2&3 and smoothed through the capacitor-resistor chain, resulting in a -4kV DC output. R1-2 are 100Ω , R3 is $25 \text{ M}\Omega$, R4 is $20 \text{ M}\Omega$, and R5 is $5 \text{ M}\Omega$.

On the primary side of the circuit, a variable transformer provides 120 VAC to two transformers wired in parallel to each other. The capacitor C₁ wired in parallel to the transformers corrects the power factor. The transformers each step up the variable transformer's voltage by a factor of 20 to the secondary side. Each transformer outputs to a half wave voltage doubler, converting the AC potential into DC. This DC output is then input into a capacitor bank to smooth out the potential.

2.4.2. Transformers

A transformer is effectively composed of two inductors. One inductor is labeled primary side and the other labeled secondary side. In our case, the primary receives a lower input

voltage and secondary outputs a higher voltage. The coils are positioned such that the center axis of each coil are the same. As current flows through the primary side it generates a magnetic field,

$$B = N \frac{\mu I}{2\pi r} \quad (2.32)$$

where N is the number of coils in the inductor, B is the magnetic field produced, μ is the permeability of the material through which the magnetic field is penetrating, I is the current within the coil and r is the radius of the coil. Since the current supplied to the coil is a result of AC potential current will change overtime causing a change in the magnetic field through a given area overtime, which is a change in magnetic flux, Φ_B . Faraday's law of induction, states that a changing magnetic field through a wire loop produces an induced voltage

$$\Delta V = - \frac{d\Phi_B}{dt} \quad (2.33)$$

where ΔV is the potential produced in the loop, and $\frac{d\Phi_B}{dt}$ is the rate of change of the magnetic flux through the coil. Applying Faraday's Law to the coils within a transformer we can find the voltage produced. We may assume that the magnetic flux through the primary coil is equal to the flux through the secondary coil, as in the transformers the coils are wound around the same core. So as a result, we have potential across both inductors given by

$$\Delta V_p = -N_p \frac{d\Phi_B}{dt} \quad (2.34)$$

in the primary coil and,

$$\Delta V_s = -N_s \frac{d\Phi_B}{dt} \quad (2.35)$$

in the secondary coil. So,

$$\frac{\Delta V_p}{\Delta V_s} = \frac{N_p}{N_s} \quad (2.36)$$

where N_p and N_s are the number of coils in the inductors on the primary and secondary sides, respectively. Thus, given the proper ratios between the number of coils on the secondary and primary sides we can step up the voltage to the desired quantity based on our input voltage.

It is important to note that when capacitors or inductors are involved in an AC circuit, the current and voltage do not peak at the same time. The period difference between the peaks is expressed in degrees as the phase difference. It is customary to use the angle by which the voltage leads the current. When voltage is applied to an inductor it resists the change in current, causing a lag in the current peak. In a capacitor, however, current is directly proportional to the charge and must lead the voltage peak to conduct charge to the capacitor. The phase difference is then given by,

$$\Phi = \tan^{-1} \left(\frac{X_L - X_C}{R} \right) \quad (2.37)$$

where R is the resistance of the system, X_L is the inductive reactance, and X_C capacitive reactance. These reactances are given by,

$$X_L = 2\pi fL = \omega L \quad (2.38)$$

$$X_C = \frac{1}{\omega C} \quad (2.39)$$

where f is the frequency in Hz, L is inductance, ω angular frequency, and C is capacitance. One can observe without the presence of a capacitor the transformers would possess the expected phase shift where voltage precedes current. For optimal power output we wish the phase difference to be zero, $X_L - X_C = 0$. This can be done with the addition of a capacitor, with a capacitance of,

$$C = \frac{1}{\omega^2 L}. \quad (2.40)$$

2.4.3. Half Wave Voltage Doubler

As depicted in Figure 9, there are two transformers present in the high voltage circuit such that they are 180° out of phase. The output of both transformers is then sent through a half wave voltage doubler. The voltage doubler is composed of a diode and a capacitor, as

highlighted in Figure 10. When the voltage from the transformer is positive, current flows through the capacitor and diode, charging the capacitor. When the voltage is negative, it is added to the capacitor voltage to produce double the peak voltage, resulting in the output shown in Figure 11. By adding an additional diode in the opposite direction, see Figure 9, the output of one transformer looks similar to the function shown in Figure 12. This output can then be smoothed by adding in a capacitor filter resulting in a DC output voltage as shown in Figure 13.

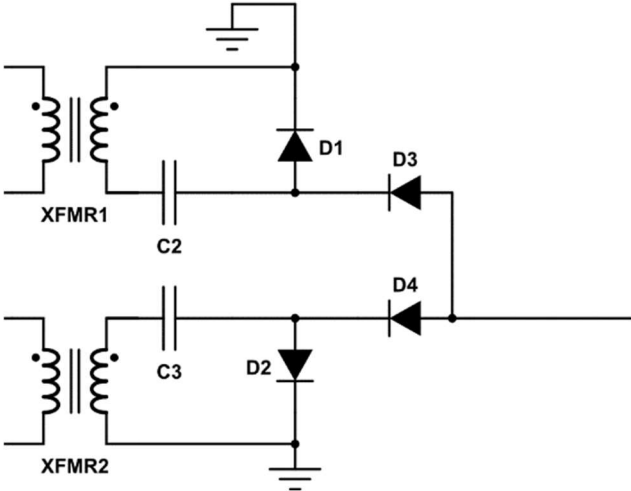


Figure 10. Isolated image of both half wave voltage doublers. Once charged, C2 and C3 shift the output voltages of each transformer such that they are always negative. Diodes 3 and 4 select the output that is most negative.

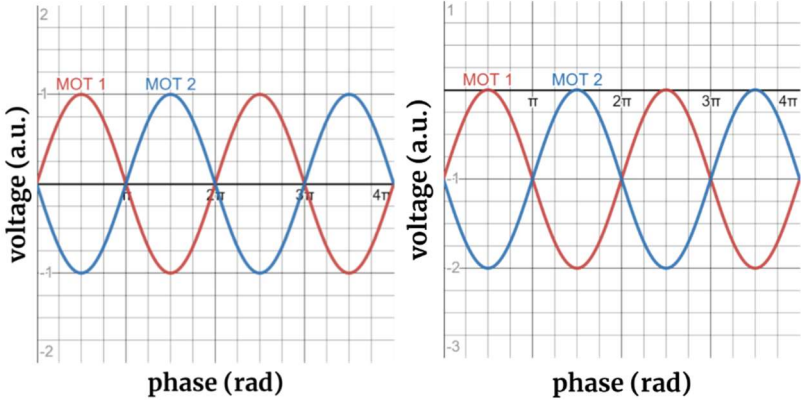


Figure 11. Plot of ideal doubler output. The wave on the left represents the voltage produced by the transformer and the wave on the right is the output of the half wave voltage doubler.

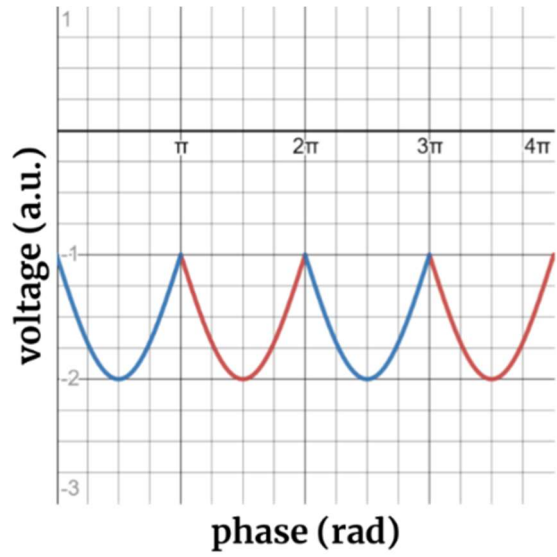


Figure 12. Plot of ideal half wave voltage doubler output.

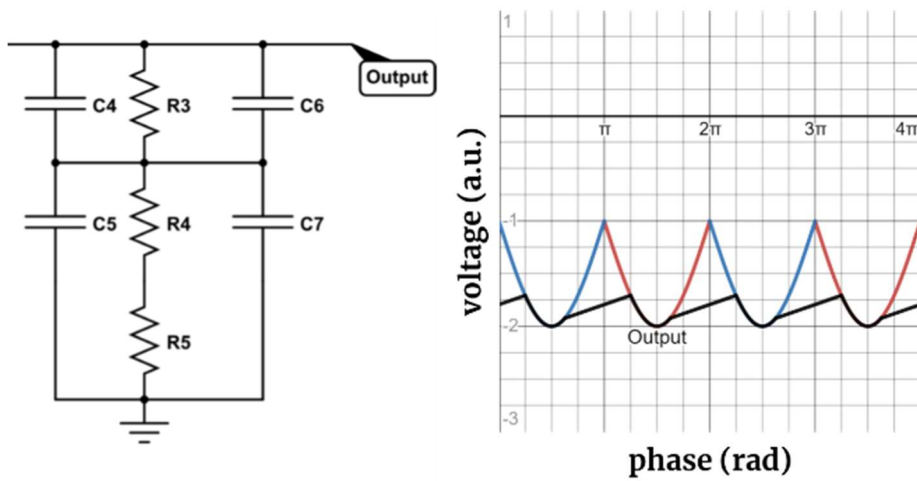


Figure 13. Diagram of ideal output of capacitor bank. Circuit diagram of capacitor filter, left. The output voltage is depicted in the right image.

Chapter 3

APPARATUS

3.1. Deposition Chamber

3.1.1. Vacuum System

The vacuum chamber is composed of an aluminum cylinder 0.91 m long and 0.28 cm in diameter, as shown in Figure 14. The chamber contains multiple mechanical feedthroughs as well as four electrical feedthroughs, along the top and sides of the chamber. Two viewing ports, which are used for viewing the internal conditions of the chamber, are also present on the chamber. One port is located in the center of the bottom, and the other on the lower half of the side. This allows the user to determine the state of the chosen metal that is to be evaporated. All feedthroughs and windows are sealed with Viton O-rings. The chamber is then initially evacuated with an Alcatel 2004a forepump and is further evacuated when the pressure within the chamber reaches an acceptable operating condition for the Pfeiffer Balzers TPU-060 turbomolecular pump. Given a sufficient operating time the vacuum system can achieve pressures as low as $1\text{e-}6$ Torr. The deposition chamber is also wrapped with thermal tape connected to a variable transformer power supply; this is to increase the rate of desorption of atoms that have adsorbed to the surfaces inside the chamber while it was vented. The chamber and tape are both coated in aluminum foil to aid in the even conduction of heat throughout the chamber.

3.2. High Voltage Circuit

A previous student, Andrew Redman [23], designed the high voltage circuit that is used to hold the filament inside the chamber at a high negative potential to accelerate the thermionic emission process.

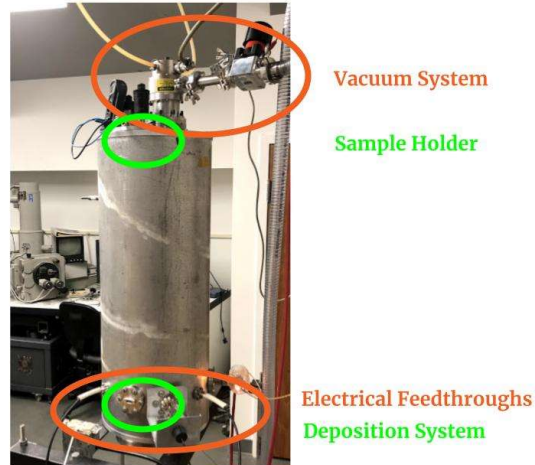


Figure 14. Image of the exterior of the deposition chamber. Thermal tape is typically wrapped around the chamber, window ports are located on the side and bottom of the chamber, electrical feedthroughs are labeled. The Balzers TPU-060 turbomolecular pump attached to the top of the deposition chamber. Note that the green labels refer to the approximate positions of components inside the chamber.

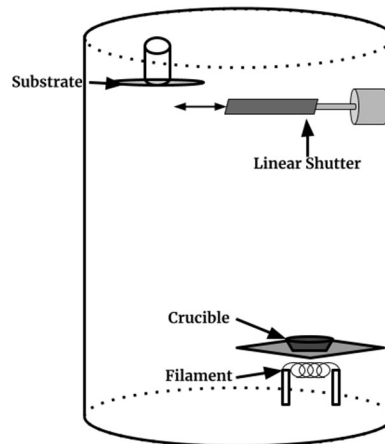


Figure 15. Diagram of the interior of the deposition chamber. The interior of the chamber is currently composed of the substrate wafer held by the sample holder, the crucible, and the crucible holder, along with the filament that is held in place by a ceramic base. The deposition rate monitor not shown, would be placed midway up the chamber attached bolted to the interior.

The circuit is composed of a variable transformer in parallel with a capacitor that powers two microwave transformers (MOT), whose outputs are input into a half wave voltage doubler composed of two diodes per MOT. The output of the half wave voltage doubler is then fed into a capacitor bank with a resistor chain that aids in converting the AC output

into DC. The resistor chain serves to ensure that potential is evenly distributed among the capacitors and to provide a voltage divider for monitoring the output voltage with an oscilloscope. The entire system is linked to a 12 VDC power supply in series with two switches that power a relay between the MOTs and the variable transformer as shown in Figure 9. This part of the system acts as a safety measure. If one of the switches is opened, meaning the power supply is no longer on a closed environment, the relay closes causing the MOTs and capacitors to be discharged through a resistor to ground.

3.3. Chamber Interior

3.3.1. Filament

The filament is held with a negative potential and current can pass through the filament, thereby allowing for the release of electrons via ionization and thermionic emission. The high negative potential is provided by a student designed high voltage power supply, as described in Section 3.3. Since the filament is held at negative potential the electrons are pushed away from the filament toward the crucible. The filament is connected via a switch and a variable resistor to a 12 V battery to provide current to the filament.

The filament is composed of 36-gauge tungsten wire, wrapped into a coil with seven coils each of radius 5 mm, whose ends are then spot welded to screws drilled into the ceramic base connected to the 12 V power supply floating at negative 4 kV.



Figure 16. Image of filament. The filament, as shown, is composed of a coiled tungsten wire, and held near the base of the crucible.

3.3.2. Crucible

The metal to be evaporated is held within a graphite crucible. The crucible is held aloft by a ceramic base that contains the filament as well as four screws which hold a metal plate above the filament. The metal plate contains a vacated area, whose shape is formed by 3 nearly concentric circles, such that the crucible contacts the plate at 3 points, allowing for minimal thermal conduction. The crucible then rests in the hole of the metal plate and rests above the filament.



Figure 17. Image of crucible and ceramic stand. The crucible, crucible stand along with the filament and ceramic base are shown in the image on the left. The crucible resting in the crucible stand is shown in the image on the right.

3.3.3. Deposition Rate Monitor

The deposition rate monitor is composed of a steel cylinder cathode and an anode, that is a coiled wire, whose functionality is described in Section 2.3. While not currently installed within the deposition chamber, the monitor will be installed later once the chamber can produce a thin film.

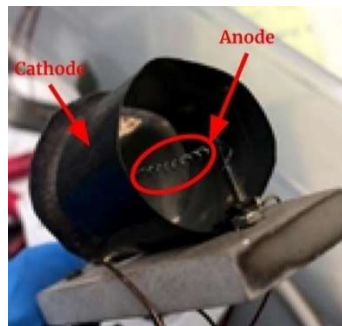


Figure 18. Images of deposition rate monitor. The steel cylinder, shown above, is grounded, and the coiled wire is connected to an oscilloscope probe, whose output can be monitored to calculate deposition rate.

3.3.4. Sample Holder

The sample holder is composed of a circular ceramic plate and three indented ceramic rods. The holder is attached to a rotary feedthrough and also wired to an electrical feedthrough at the top of the chamber. The output of the electrical feedthrough is monitored via a multimeter measuring resistance. Wire extends from leads of the feedthrough to the edges of where the substrate rests such that when no metal is deposited on the substrate the multimeter registers an open loop. However, when metal is deposited the multimeter registers the resistance of the film and the operator can tell a film has been produced.

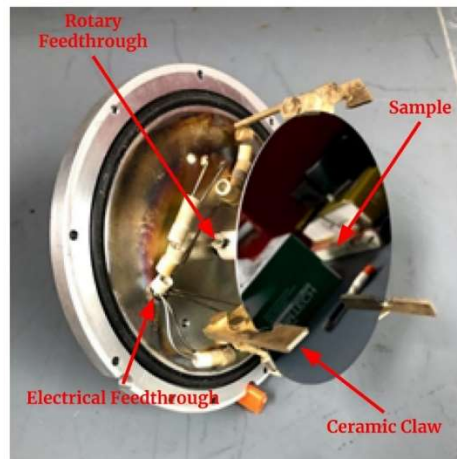


Figure 19. Image of Sample Holder. The sample holder is composed of three ceramic claws attached to a rotary feedthrough, thereby allowing the rotation of the sample in the deposition process.

3.3.5. Motion Feedthroughs

A set of linear and rotary feedthroughs are present on the chamber. The linear feedthrough allows for translation in the XY plane of the chamber. The linear feedthrough has a stepper motor for controlled motion. Its primary use will be a primary component of a linear shutter, attached to a retractable plate that can be utilized to produce a thin film with varying thickness. Rotary feedthroughs will be utilized in the rotation of the sample during the deposition process to produce radial thickness gradients within the film. Additionally, a rotary feedthrough will have a 10 cm circular shutter attached, to quickly uncover and cover the sample by hand at the beginning and end of deposition.

Chapter 4

CONCLUSION

4.1. Chamber Operability

Presently the Houghton college deposition chamber is ready to produce a thin metal film. However, we have no means of controlling the temperature of the substrate or the thickness of the film. Additionally, the chamber is not capable of variation of thickness within the film. However, these means should be achievable.

4.1.1. Substrate Temperature Control

Previous designs to regulate the temperature of the substrate were developed, however they have been temporarily removed due to complications with the sample holder. Thin wire was laced and interwoven into the ceramic plate that holds the substrate. This wire was then connected to the leads of an electrical feedthrough that the sample holder is connected to. An external power supply can then be connected to the feedthrough to provide current to the wire and produce thermionic emissions, which then elevate the temperature of the substrate. This way the substrate could be held at a higher temperature than the internal temperature of the chamber and films could be produced such that we could analyze the properties of a thin metal film deposited on a substrate with a higher temperature than the environment deposited in.

4.1.2. Deposition Rate Monitor

As mentioned in Section 3.3.3, a deposition rate monitor has been manufactured for the deposition chamber, but it has not been installed or calibrated. Upon installation, the operator of the chamber would be able to determine the rate of deposition after a few calibrating trials. With the rate monitor fully functional, we can more accurately produce films of a desired thickness as the thickness of the film could be regulated by knowing the deposition rate and how long the deposition process occurred for.

4.1.3. Linear Shutter

Designs for the linear shutter are still in development. However, in conjunction with the deposition rate monitor, the linear shutter would allow for the production of thin films with a thickness gradient. The linear shutter would be composed, of a metal plate completely covering the substrate that is fixed to a linear feedthrough, such that the plate could be completely pulled away to reveal the film. A simplified diagram of the linear shutter is shown in Figure 15. During the deposition process the film could be retracted and then slowly closed at a given rate, thereby allowing for the production of a thickness gradient within the thin film.

References

-
- [1] Guericke, O. V. *The New Experiments of Otto Von Guericke*. (1672).
- [2] Sprengel, H. Reseaches on the Vacuum. Chem. Soc. of London **3** 9 (1865).
- [3] Gaede, W. U.S. Patent No. 534,518. (Aug. 5,1913.)
- [4] J. Moore *et. al.*, Building Scientific Apparatus. Avalon Publishing, (2002).
- [5] M. Audi, Ion pumps, Vacuum **37** 629 (1987)
- [6] W. Becker, The Turbomolecular pump, its design, operation, and theory. **16** 625 (1966).
- [7] L. B Hunt, The Early History of Gold Plating. (1840)
- [8] O. Younes, Electroplating of Amorphous Thin Films of Tungsten. Johnson Matthey & Co Limited (2001).
- [9] A. G. Emslie, Flow of a Viscous Liquid on a Rotating Disk. J. App. Phys. **29** 858 (1958).
- [10] J. Griffin, <https://www.ossila.com/pages/spin-coating>. (6/7/21)
- [11] Haubner, R. The history of hard CVD coatings for tool applications at the University of Technology Vienna. International Journal of Refractory Metals & Hard Materials, **41** 22 (2012).
- [12] Kahler, H. The Crystalline Structures of Sputtered and Evaporated Metallic Films. American Physical Society, **18** 210(1921).
- [13] H. M. O'Bryan, Evaporation Technique for High Refractory Substances. Review of Sci. Instr. **5** 125 (1934).
- [14] G. R. Giedd, *et. al.* Evaporation Rate Monitor. Review of Sci. Instr. **31** 773(1960).
- [15] S.B. Lee, *et al.* Grain boundary faceting and abnormal grain growth in nickel. Metall Mater Trans **31**, 985 (2000).
- [16] R. Carel, Grain Growth and Texture Evolution. MIT (1995).
- [17] P. Kumar, Effect of microstructural evolution on magnetic properties of Ni thin films. Mater. Sci., **32** 263 (2009).
- [18] S. R. Baker, *et. al.* Texture transformations in Ag thin films. Elsevier **61** 7121 (2013).
- [19] Petrasonnweber-Ribic. Kinetics and driving forces of abnormal grain growth in thin Cu films. Acta Materialia. **60** 2397 (2012).
- [20] E. A. Ellis, Driving forces for texture transformation in thin Ag films. Acta Materialia **60** 495 (2016).
- [21] De, Daim. Modification of Richardson-Dushman Equation, variation of thermionic emission constants, temperature variation of work function in metals. (2012).
- [22] J. Safarian, Vacuum Evaporation of Pure Metals. Metallurgical and Materials Transactions, **44** 747 (2012).
- [23] R. Redman, Development and Integration of a low cost, High Voltage Power Supply into a thin film Deposition System. Houghton College (2017).